Available online at www.sciencedirect.com
SCIENCE DIRECT®

Journal of the European Ceramic Society 24 (2004) 3287–3294
www.elsevier.com/locate/jeurceramsoc

Manufacture and examination of C/Si_3N_4 nanocomposites

Cs. Balázsi[a,*], F.S. Cinar[b], O. Addemir[b], F. Wéber[a], P. Arató[a]

[a]*Ceramics and Refractory Metals Laboratory, Research Institute for Technical Physics and Materials Science, Hungarian Academy of Sciences, 1121 Konkoly-Thege út 29-33, Budapest, Hungary*
[b]*Prof. Adnan Tekin High Technological Ceramics and Composites ResearchCenter, 80626 Maslak, Istanbul, Turkey*

Abstract

C/Si_3N_4 nanocomposites have been prepared through carbon black nanograins, graphite micrograins addition to silicon nitride starting powder. The role of excess oxygen was examined by oxidising the alpha silicon nitride starting powder. For nanocomposite processing sinter-HIP and hot press have been applied. Bending strength and elastic modulus have been found to be influenced by amount of carbon black and graphite introduced in silicon nitride matrix. In the case of HIP samples a desintering process was observed. During pressure-less sintering step the structure retained the α-Si_3N_4 phase, after second sintering step new phase(s) appeared. Hot pressed samples with a higher α-Si_3N_4 phase contribution showed considerable improvement of hardness.

Keywords: Nanocomposites; Porosity; Si_3N_4; Sintering; Strength

1. Introduction

Ceramics based on silicon nitride are well-known as low density materials with high strength and toughness. With these combination of properties silicon nitride based ceramics are an ideal candidate for several structural applications. However, applications to higher temperatures (greater than 1000 °C) face difficulties due to degradation of grain boundary phases. Generally, there are two ways to improve the mechanical properties of ceramics: controlling the microstructure and preparation of composite. Lately, by in-situ tailoring the microstructure, new observations were performed on structural and morphological development on silicon nitride ceramics in order to understand the governing principles of sintering processes.[1,2] In this way, through formation of tough interlocking microstructure (consisting of elongated β-Si_3N_4 grains) mechanical properties may be improved. In the other hand, physical and mechanical properties of silicon nitride ceramics can be improved through nanocomposite processing.[3–5] To increase the fracture toughness, incorporation of various energy-dissipating components into ceramic matrices have been performed.[6] The second phases act as bridging elements at the grain boundaries, thus hindering grain boundary sliding. These components can be introduced in whisker, platelets, particles or fibre forms. Depending on processing route micro/nano or nano/nano type microstructures can be synthesised. Recently, silicon nitride–silicon carbide nanocomposites were developed, which retained high strength and good oxidation resistance up to 1400 °C.[7,8] Moreover, through nanocomposite processing not only the high temperature properties may be improved, but high-performance structural materials can be synthesised. From literature work, are known several methods for obtaining porous ceramics, such as partial sintering[9] or using sintering additives with high melting points to hinder the sintering process.[10] It was reported that by small carbon addition high porous silicon nitride composites with low shrinkage have been realised.[11] This process involved the formation of SiC particles at the grain boundaries, which inhibited the rearrangement of Si_3N_4 particles during sintering, assuring high porosity. A method for producing porous silicon nitride having high strength and low thermal conductivity by adding β-Si_3N_4 crystal seeds was presented by Toriyama et al.[12,13] A carefully control of oxidation process of Si_3N_4 that contains organic binder as source of carbon can lead to porous ceramic with high strength.[14] Addressing to these critical points, we performed the preparation and examination of carbon added silicon nitride ceramic matrix composites. Results about structural, morphological measurements and mechanical properties are presented.

* Corresponding author. Tel.: +36-1-392-2222; fax: +36-1-392-2226.
E-mail address: balazsi@mfa.kfki.hu (C.. Balázsi).

0955-2219/$ - see front matter © 2003 Elsevier Ltd. All rights reserved.
doi:10.1016/j.jeurceramsoc.2003.10.021

2. Experimental method

2.1. Materials

Details about sample preparation can be followed in Table 1. The compositions of the starting powder mixtures of the eight materials were the same: Si_3N_4 (Ube, SN-ESP), Al_2O_3 (Alcoa, A16) and Y_2O_3 (H. C. Starck, grade C). In addition to batches carbon black (Taurus Carbon black, N330, average particle size between ~50 and 100 nm), graphite (Aldrich, synthetic, average particle size 1–2 μm) were added. Samples of batch 683 were prepared with surface modified alpha silicon nitride. Oxidation of the surface of powders was performed at 1000 °C in air for 150 h. The powder mixtures were milled in ethanol in a planetary type alumina ball mill. Each batch contains approximately 1 g alumina as contamination from balls and jars. The batches were sieved with 150 μm mesh. Powder samples were passed to FTIR examinations.

2.2. Sintering methods

Samples for HIP (ABRA), were compacted by dry pressing at 220 MPa. The materials were sintered at 1700 °C in high purity nitrogen by a two-step sinter-HIP method using BN embedding powder. First, some of the samples were sintered without applying pressure. In second step, the samples from first sintering step (serving as reference samples) were re-introduced in the HIP together with the rest of examined samples. Then, a pressure of 2 MPa were applied for 1 h. The dimensions of the as-sintered specimens were approximately 3.5×5×50 mm.

Samples for HP (CENTORR Vacuum Industries) were prepared as follows. After 10^{-4} Torr vacuum, at 20 °C, nitrogen gas were introduced at 1 atm. Heating rate was 20 °C/min till 1800 °C. At 1000 °C uniaxial pressure of 2.8 MPa was applied. From 1400 °C the pressure was increased step by step to 40 MPa. At 1800 °C the pressure was kept at 40 MPa and was applied for 2 h. The samples were cooling down together with furnace.

Table 1
The preparation conditions and composition of starting powder mixtures

Batch	Composition (wt.%)			Added carbon (wt.% to batch)		Milling (in ethanol) (h)
	Si_3N_4	Al_2O_3	Y_2O_3	Carbon black	Graphite	
HIP						
642	90	4	6	–	–	3
644	90	4	6	23	–	150
645	90	4	6	–	23	150
683	90	4	6	23		3
HP						
713	90	4	6	–	–	3
714	90	4	6	1		3
715	90	4	6	10		3

2.3. Microstructural observations and mechanical tests

After sintering the weight of the samples were determined. All surfaces of the test bars were finely ground on a diamond wheel, and the edges were bevelled. The direction of both the diamond grinding and of the bevelling was parallel with the bar lengths. The density of the as-sintered materials was measured by the Archimedes method. To identify the crystalline phases X-ray diffraction of Cu K_α radiation was applied by a Philips PW 1050 diffractometer. Infrared absorption spectra were taken by BOMEM MB-102 FTIR spectrophotometer equipped with deutero-triglicine-sulfate detector, at a resolution of 4 cm^{-1}, in the range of 400–4000 cm^{-1}; 2 mg/g KBr pellets were used. Morphology of the solid products was studied by scanning electron microscopy, with a JEOL-25 microscope. The elastic modulus and the four-point bend strength were determined by a bending test with spans of 40 and 20 mm. Three-point strength was measured on broken pieces with span 20 mm. Hardness measurements were performed on micro Vickers Model LL, Tukor Tester, by applying 1 kg load.

3. Results and discussion

3.1. Milling an oxidation

The mixing of powders was monitored step by step by infrared observations. Infrared spectroscopy measurements are presented on Fig. 1. Samples from batches

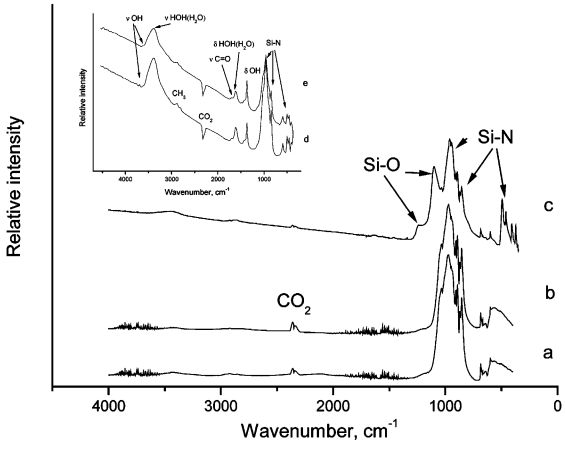

Fig. 1. FTIR spectra of milling products: (a) resulting mixture after 150 h activation, batch 644; (b) resulting mixture after 150h activation, batch 645; (c) mixture after 3 h milling, batch 683. On the inset: (d) mixture after 3 h activation, batch 713; (e) mixture after 3 h activation, batch 715.

644 and 645 are characterized mainly by Si–N vibration modes (Fig. 1a and b). In the case of batch 683 (Fig. 1c) due to surface oxidation of alpha silicon nitride powders vibration modes of Si–O bonds appeared at 1250 and 1100 cm^{-1}. In the inset infrared spectras of samples 713 and 715 are presented (Fig. 1d and e). These spectras are characterized by the same vibration modes. However, some of the vibration modes of ethanol can be recognized as OH, H_2O, CH_3 and C=O stretching (ν) and bending (δ) vibrations [15–18].

After performing the mechanical activation of powder mixtures, for HIP samples, rectangular bars were obtained by dry pressing at 220 MPa. The as-obtained samples were oxidized for 2 h. Oxidation at different temperatures resulted in samples with different carbon content as presented in Fig. 2. The carbon removal was very fast in the case of batch 683. The behavior of carbon black (batch 644) and graphite (batch 645) added silicon nitride matrix was found to be significantly different regarding the oxidation process. From 450 °C up to 600 °C the carbon black content has a decreasing tendency, at 600 °C was 0.4 wt.%. At this stage the graphite content is around 10 wt.%. Above this temperature the graphite content has also a decreasing tendency with increasing temperature. Continuing the oxidation process above 800 °C, according to weight losses we obtained almost a carbon free structure. During oxidation process carbon is released as CO or CO_2 gas while the surface of α-Si_3N_4 in the compacts may be also oxidized (case of batches 644 and 645), but we have not observed Si–O bond evolving on the infrared spectra of compacts.

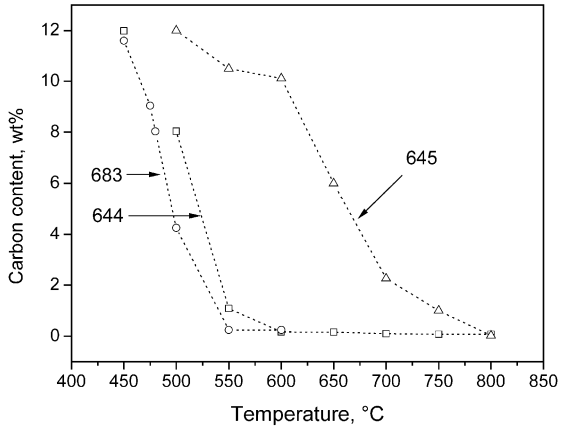

Fig. 2. Samples from batches 644, 683 and 645 with different carbon content after oxidation in atmosphere. Average values of four samples are presented.

3.2. Morphological observations

Morphological study was performed after sintering by scanning electron microscopy. In Fig. 3a and b the microstructure and the fracture surface of reference sample (642) consisting of uniform grains is shown. The structures characterized by high carbon content can be seen Fig. 3c and d. A totally different morphology is developing in the case of samples from batch 683 (Fig. 4a and b). These samples characterized by minimal (0.56 wt.%) respective with considerable high (10.62 wt.%) carbon content after oxidation are showing new crystal facets (similar to Ref. 23) in both cases after sintering.

Sharply different microstructure, well developed β-Si_3N_4 grains evolved in the case of sample (from batch 644) with no carbon content after oxidation at 800 °C (Fig. 5). Low magnification shows macro- and micropores present in structure (Fig. 5a). In preferred sites, mainly on the cavity surfaces huge β-Si_3N_4 grains developed with 2–3 μm thickness, 10 μm length (Fig. 5c). However, the characteristic microstructure consist of β-Si_3N_4 crystals with 3–4 μm length and submicron thickness, as in Fig. 5b. The growing in excess of β-Si_3N_4 grains can be related to huge pores present in structure induced by oxidation through elimination of the adhered carbon phases, which resulted during milling.[15] The highly porous sample may exhibit preferred growing sites, surfaces that can contact the reaction gases during sintering more easily than more compact ones (e.g. batch 642). If we compare the microstructure of the samples with high carbon black and graphite

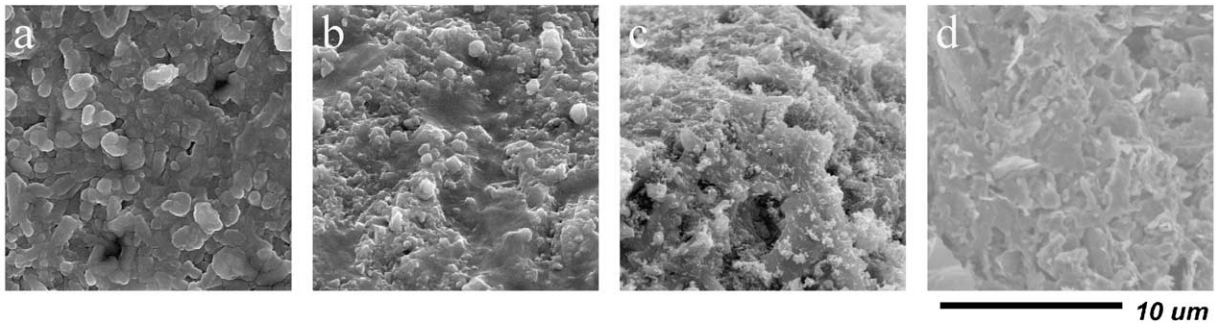

Fig. 3. Micrographs of the samples after sintering process: (a) reference sample (642); (b) fracture surface of the reference sample; (c) sample from batch 644, with 11.9 wt.% carbon content after oxidation at 450 °C (see Fig. 2); (d) sample from batch 645, with 12 wt.% graphite content after oxidation at 500 °C.

content (Fig. 3c and d) with the carbon free sample after oxidation, we should remark that only in the later case developed such a huge β-Si_3N_4 grains.

In Fig. 6a the microstructure of hot pressed HP sample consisting of submicron grains (batch 713) can be seen. Fig. 6b shows the polished surface of sample with cracks propagated by the Vickers indentation. The crack deflection (zigzagged crack) appears due to rod-like grains contained in this specimen. This may cause an increase in fracture toughness.[20]

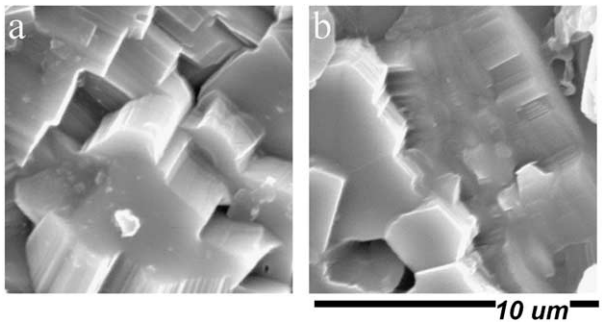

Fig. 4. Micrographs of the samples after sintering process: (a) sample from batch 683, with 0.56 wt.% carbon content after oxidation at 550 °C; (b) sample from batch 683, with 10.62 wt.% carbon content after oxidation at 480 °C. Bar: 10 μm for all of the samples.

3.3. Mechanical properties and structural observations

Relation between apparent density and modulus of elasticity of samples containing carbon (batches 644, 645, 683, 714, 715) and reference (642 and 713) carbon free samples after sintering are presented on Fig. 7. The 642 HIP reference samples are characterized by higher apparent density and higher modulus than samples with carbon content. Linearly fitted dashed line was added to Fig. 7 from Ref. 9. This line has been produced to study partial and final sintering processes of silicon nitride. On Fig. 7 it is shown that with changing carbon content in the specimens resulted in the similar porous structures (with low densities) as in the case of partial sintering. The slope of the regression lines of samples 644, 683 and 645–the full lines of Fig. 7—is similar, this value is lower than was in the case of Ref. 9. As conclusion can be drawn that samples 644 and some samples from 683 at low densities have higher modulus values than samples from Ref. 9. In the range of 1.5–2.1 g/cm^3 the 683 samples have higher modulus than 644 samples. Hot pressed samples, with and without carbon addition (713 and 714) marked with circles, are characterized by higher densities and modulus than HIP samples.

A desintering process (decreasing of density) was observed during two-step HIP sintering process, as

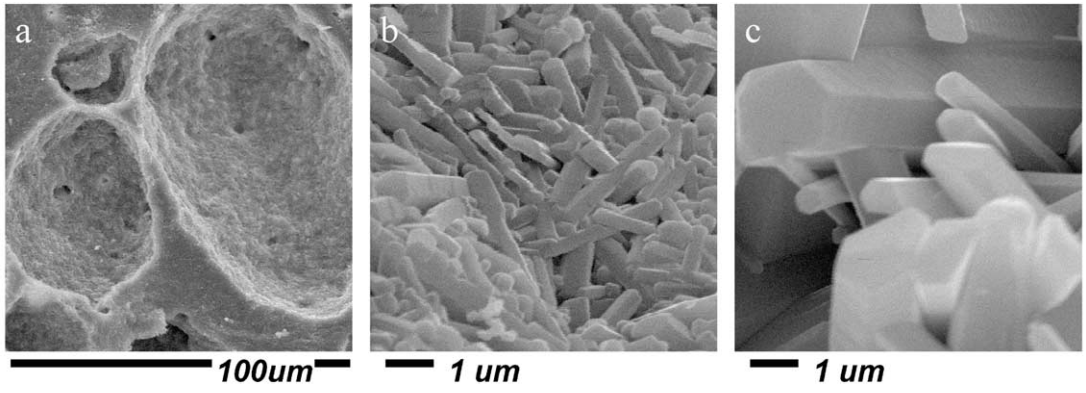

Fig. 5. Micrograph of porous sample from batch 644, with no carbon content after oxidation at 800 °C: (a) macro- and micro-pores are present in structure; (b) characteristic microstructure with β-Si_3N_4 grains; (c) well developed β-Si_3N_4 grains.

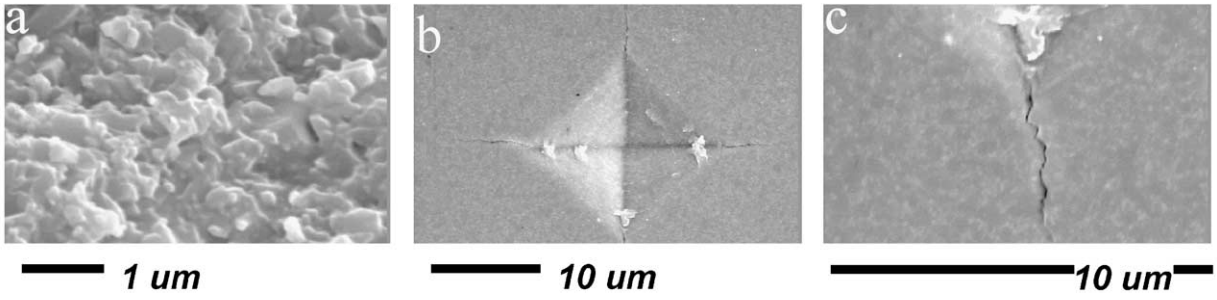

Fig. 6. Micrographs of hot pressed reference sample (batch 713): (a) submicron grains of hot developed after hot pressing; (b) cracks propagated by the Vickers indentation; (c) zigzagged cracks.

shown in Fig. 8. The starting points of arrows present the first sintering step without any pressure applied. The ends of arrows present the second sintering step with 2 MPa pressure applied. The desintering process was observed for reference sample (642) and for batches 644 (samples containing ~0.1 wt.% carbon after oxidation) and 645 (samples with no graphite content after oxidation) as well. A very similar desintering phenomenon was described by Hwang et al. in the case of gas-pressure sintering.[21] The decrease of density was ascribed to chemical dissolution of nitrogen into oxynitride melts assisted by high pressure and presence of boron nitride phases. An interesting remark should be added to desintering observation presented on Fig. 8. In the case of reference sample (642) we have the similar decrease of density as in the case of batches 644 and 645, but the effect on modulus of elasticity is reversed. An accompanying phase transformation to desintering process can be seen on Fig. 9.

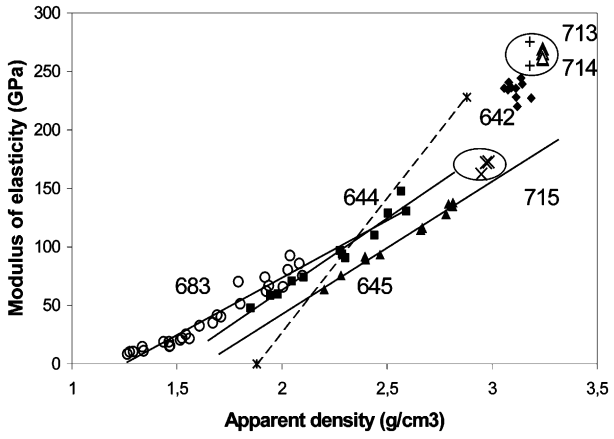

Fig. 7. Relation between apparent density and modulus of elasticity after sintering. Sinter—HIP samples: reference 642, with carbon addition 644, 645. HP samples (marked with circles): reference 713, and with carbon black addition 714, 715.

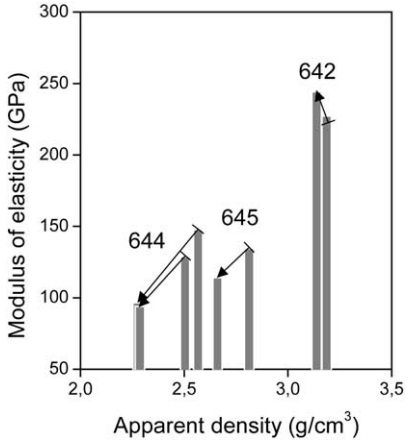

Fig. 8. The effect of desintering observed during two-step sintering process (without and with pressure applied) on reference sample (from batch 642), two samples with carbon content ~0.1 wt.% carbon content after oxidation at 800 °C, from batch 644 and one sample from batch 645, with no graphite content after oxidation at 800 °C.

On Fig. 9a the X-ray diffractogram of reference sample is presented after HIP sintering at 1700 °C, nitrogen atmosphere and without applying pressure. The structure consist of β-Si_3N_4 and α-Si_3N_4. After the second sintering step (Fig. 9b) mostly the reflection of β-Si_3N_4 can be recognized. At $d=0.3041$ nm however, a peak has appeared. This reflection may be attributed to δ-$Y_2Si_2O_7$ phase (JCPDS-PDF 21-1460). In Fig. 9c the reflections of sample from batch 644 can be seen after first sintering step. The structure consist of β-Si_3N_4 and α-Si_3N_4 as in case of reference sample. In addition to this reflections at $d=0.3613$ nm and $d=0.3041$ nm can be observed which may be attributed to δ-$Y_2Si_2O_7$ reflections. Some reflections of SiC (JCPDS-PDF 31-1231) can be observed as well. After the second sintering step the structure is converting to β-Si_3N_4 phase, but retains some of the possible δ-$Y_2Si_2O_7$ reflections ($d=0.3613$ nm and $d=0.3041$ nm) and some of the α-Si_3N_4 reflections ($d=0.2259$ nm, 0.2619 and 0.280 nm).

In Fig. 10 the X-ray diffractogram of a HIP sintered reference sample and diffractograms of specimens from batch 683 can be seen. The structure consists of β-Si_3N_4 in the case of reference sample. In Fig. 10b remaining reflections of β-Si_3N_4 can be recognized. Main lines of a new phase (Si_2N_2O) appeared at $d=0.466$ nm, $d=0.444$ nm, $d=0.336$ nm, $d=0.26$ nm, $d=0.242$ nm and $d=0.239$ nm. On Fig. 10c the Si_2N_2O is the main phase with additional $Si_3Al_3O_3N_5$ lines at $d=0.384$ nm and $d=0.332$ nm.

In Fig. 11 the X-ray diffractograms of HP sintered samples are shown. As in the case of HIP samples at $d=0.3041$ nm, a diffraction peak related to δ-$Y_2Si_2O_7$ phase appeared (Fig. 9). This peak is present on the all of the HP structures, as on the carbon free structure too, but in the case of 1 wt.% carbon content (batch 714) represents the highest peak (Fig. 11b). At the end of the sintering all of the specimens have β-Si_3N_4 and α-Si_3N_4 as main components. This may explain the high hardness value (22 Gpa) obtained for carbon free sample (batch 713). Generally, silicon nitride samples produced in our laboratory with HIP method are characterized by a hardness value high as 18.5 Gpa.[22]

As observed by X-ray measurements after sintering the conversion α→β-Si_3N_4 is completed only in the case of HIP samples. In the case of surface oxidized samples glassy phases are evolving. The formation of SiC phase have been observed only in the case of presented HIP experiments, as we expected from earlier works.[11,19,24] However, in our case the SiC act as an intermediate phase in the reactions as discussed in elsewhere.[25] In the presence of silicon-rich liquid, at certain nitrogen pressure the decomposition of silicon carbide cannot be avoided.[26]

A comprehensive view about the carbon content effect to strength can be seen in Fig. 12. Samples with added carbon (644, 645, 714, 715) due to lower densities, show lower values for strength as compared with 642, 713 reference samples. The porous sample presented in Fig. 5 has a modulus 97 GPa at 2.276 (g/cm^3) apparent density and 130 MPa value for three point bending strength. As can be seen on the graph and inset the hot pressed samples in all of the cases are characterized by higher bending strengths than sinter-HIP specimens.

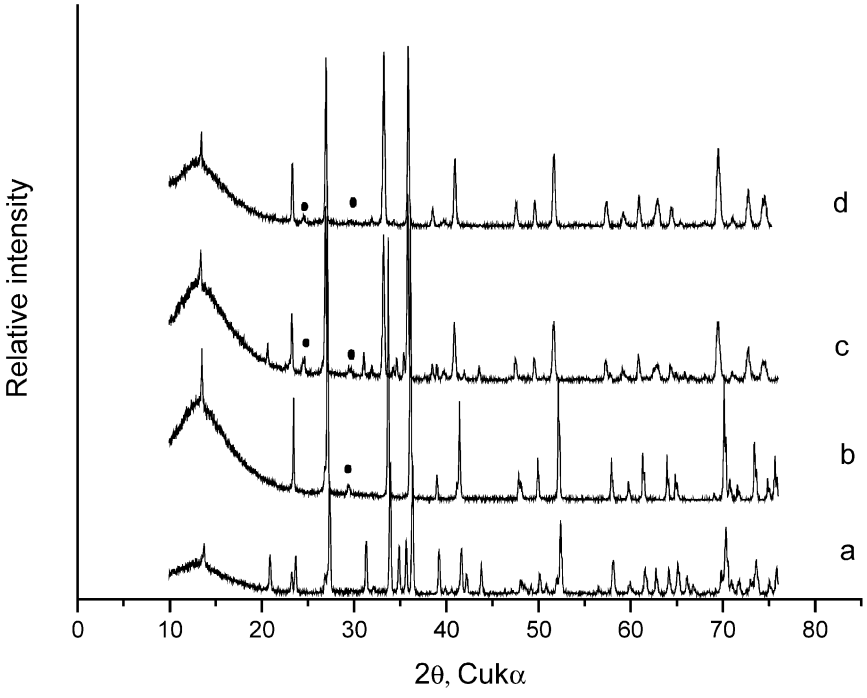

Fig. 9. X-ray diffractograms of one and two step sintered samples: (a) reference sample (from batch 642) sintered without pressure; (b) reference sample (642) sintered under pressure; (c) carbon added (644) sample first step sintered; (d) carbon added sample (644) after two-step sintering. Black points mark new phase(s).

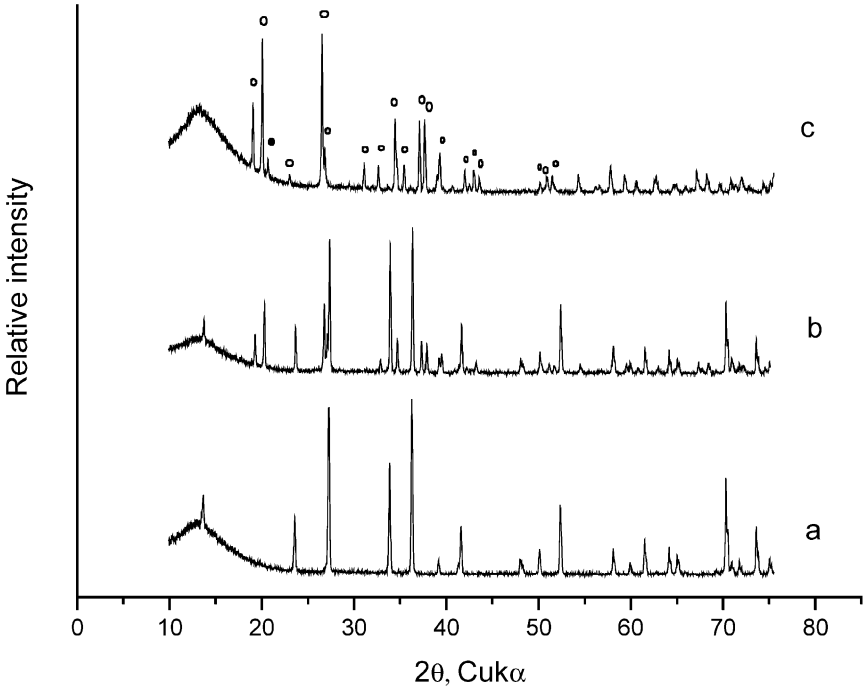

Fig. 10. X-ray diffractograms of sintered samples: (a) reference sample (642); (b) sample with 10.62 wt.% C after oxidation (683); (c) sample with 0.56 wt.% C after oxidation (683).

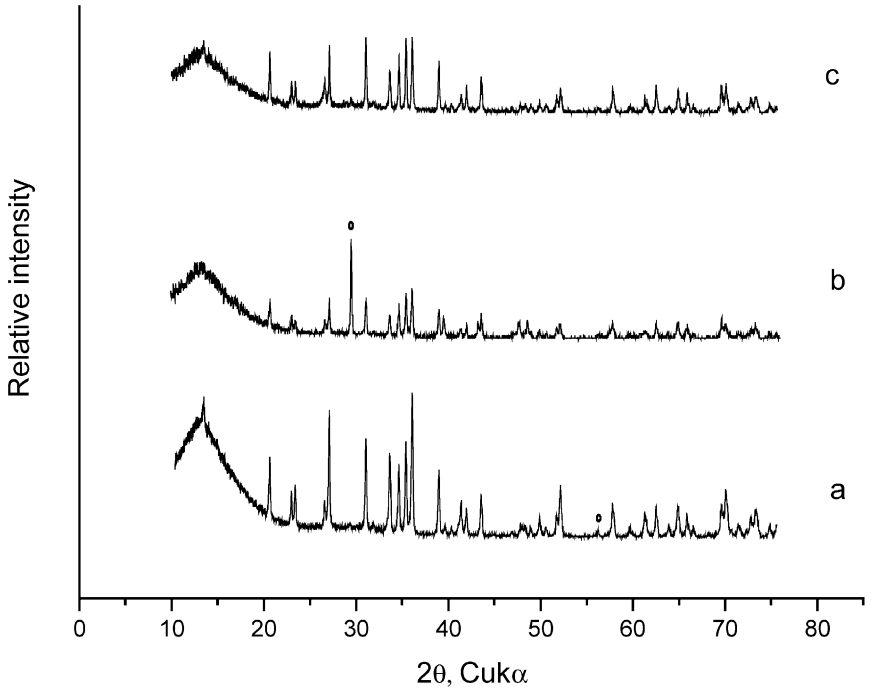

Fig. 11. X-ray diffractograms of hot pressed samples: (a) reference sample (713); (b) sample with 1 wt.% carbon (714); (c) sample with 10 wt% carbon (715).

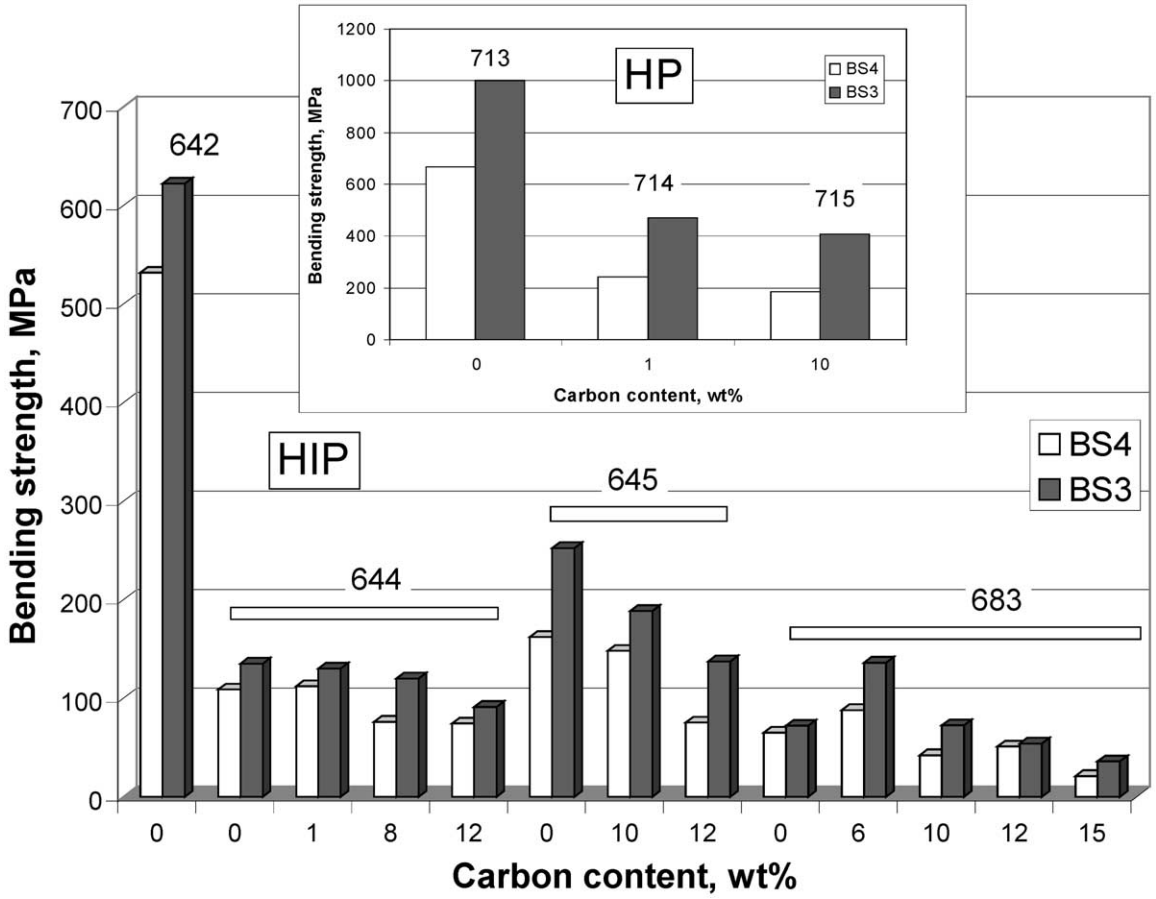

Fig. 12. Relation between carbon content and four point bending strength (BS4) and three point bending strength (BS3). Carbon contents for samples 644 and 645 resulted from oxidation process as in Fig. 3. Hot pressed composites are characterized by 1 and 10 wt.% carbon content as in Table 1.

4. Conclusion

The structure and properties of silicon nitride ceramics may be improved by adding carbon nano- and micrograins or modifying the surface of starting powders. The milling products of added carbon black and graphite have the same vibration modes on infrared spectra. Carbon addition resulted in porous samples, thus has the same advantages as partial sintering or addition of sintering aids. In the initial stage of sintering the carbon addition has a beneficial role to the modulus of elasticity. Compared with partial sintering, however, above a certain value carbon content has a detrimental role to modulus. A desintering process was observed. During desintering process the $\alpha \rightarrow \beta$-Si_3N_4 was completed. The porous samples suffered a decrease, the reference sample had an increase of modulus. The porous samples have 20–100 μm macro- and 1–2 μm microporosity and consist of huge β-Si_3N_4 grains. In the case of specimens with oxidized surface glassy phases appeared, the morphology is independent from carbon content of samples after oxidation. The structure of hot pressed specimens consist of α and β-Si_3N_4, therefore an increase of hardness was observed.

Uncited references

Refs 19 and 23 are not cited in the text.

Acknowledgements

Csaba Balázsi thanks for OTKA Postdoctoral Research Grant (D38478) and János Bolyai Research Grant. Support from Hungarian State Eötvös Fellowhsip is greatly acknowledged. This work was supported by OTKA Foundation (No. T43704).

References

1. Shen, Z., Zhao, Z., Peng, H. and Nygren, M., Formation of tough interlocking microstructures in silicon nitride ceramics by dynamic ripening. *Nature*, 2002, **417**, 266–269.
2. Thompson, D. P., Cooking up tougher ceramics. *Nature*, 2002, **417**, 237.
3. Sternitzke, M., Structural ceramic nanocomposites. *Journal of the European Ceramic Society*, 1997, **17**, 1061–1082.
4. Iwamoto, Y., Kikuta, Ko-ichi. and Hirano, Shin-ichi., Si_3N_4–SiC–Y_2O_3 ceramics derived from yttrium-modified block copolymer of perhydropolysilazane and hydroxy-polycarbosilane. *J. Mat. Res.*, 1999, **14**(15), 1886–1895.
5. Hermann, M., Schubert, C., Rendtel, A. and Hübner, H., Silicon nitride/silicon carbide nanocomposite materials: I, fabrication and mechanical properties at room temperature. *J. Am. Ceram. Soc.*, 1998, **81**(5), 1095–1108.
6. Derby, B., Ceramic nanocomposites: mechanical properties. *Cur. Op. Solid State Mat. Sci.*, 1998, **3**, 490–495.
7. Niihara, K., New design concept of structural ceramics-ceramic nanocomposites. *J. Jpn. Ceram. Soc.*, 1991, **99**(10), 974–982.
8. Rendtel, A., Hübner, H., Hermann, M. and Schubert, C., Silicon nitride/silicon carbide nanocomposite materials: II, hot strength, creep and oxidation resistance. *J. Am. Ceram. Soc.*, 1998, **81**(5), 1109–1120.
9. Arató, P., Besenyei, E., Kele, A. and Wéber, F., Mechanical properties in the initial stage of sintering. *J. Mat. Sci.*, 1995, **30**, 1863–1871.
10. Yang, J-F., Deng, Z-Y. and Ohji, T., Fabrication and characterisation of porous silicon nitride ceramics using Yb_2O_3 as sintering additive. *Journal of the European Ceramic Society*, 2003, **23**, 371–378.
11. Yang, J-F., Yhang, G-J. and Ohji, T., Fabrication of low-shrinkage, porous silicon nitride ceramics by addition of a small amount of carbon. *J. Am. Ceram. Soc.*, 2001, **84**(7), 1639–1641.
12. Toriyama, M., Hirao, K., Brito, M. E., Kanzaki, S. and Shigegaki, Y. US Patent, 5,935,888.
13. Hirao, K., Brito, M. E., Toriyama, M., Kanzaki, S., Imamura, H., Hirai, T. and Shigegaki, Y. US Patent, 5,968,426.
14. Kawai, C., Matsuura, T. and Yamakawa, A. US Patent, 5,780,374.
15. Balázsi, Cs., Wéber, F. and Arató, P., Investigation of C/ Si_3N_4 nanocomposites. *Mat.-wiss. u. Werkstofftech*, 2003, **34**, 332–337.
16. Balázsi, Cs., Wéber, F. and Arató, P. Examination of C/Si_3N_4 nanocomposites. *Key Eng. Mat.* (submitted for publication).
17. Balázsi, Cs., Kasztovszky, Zs. and Wéber, F. Preparation and compositional analysis of carbon black containing silicon nitride composites. In *Proceedings TRANSCOM'03*, Zilina, June 2003.
18. Nakamoto, K., *Infrared Spectra of Inorganic and Coordination Compounds*. Wiley-Interscience, New York, 1963.
19. Zemanova, M., Lecomte, E., Sajgalik, P. and Riedel, R., Polysilazane derived micro/nano Si_3N_4/SiC composites. *Journal of the European Ceramic Society*, 2002, **22**, 2963–2968.
20. Zhilinska, N., Zalite, I., Grabis, J. and Kladler, G., High temperature construction materials on the basis of nanodisperse silicon nitride. *Mat.-wiss. u. Werkstofftech*, 2003, **34**, 327–331.
21. Hwang, S-L., Becher, P. E. and Lin, H. T., Desintering process in the gas pressure sintering of silicon nitride. *J. Am. Ceram. Soc.*, 1997, **80**(2), 329–335.
22. See: http://www.mfa.kfki.hu/.
23. Wang, C., Emoto, H. and Mitomo, M., Nucleation and growth of silicon oxynitride grains in a fine-grained silicon nitride matrix. *J. Am. Ceram. Soc.*, 1998, **81**(5), 1125–1132.
24. Hnatko, M., Sajgalik, P., Lences, Z., Monteverde, F., Dusza, J., Warbichler, P. and Hofer, F., Low cost SiC/ Si_3N_4 nanocomposites. *Key Eng. Mat.*, 2002, **206–213**, 1061–1064.
25. Cinar, F. S., Van der Hejde, J. C. T., Terpstra, R. A. and Tekin, A., The preparation of β sialon from kaolin by carbonitrothermic reduction. *High Temp. Mat. Proc. (London)*, 1996, **15**(1–2), 97–101.
26. Kennedy, T., Poorteman, M., Cambier, F. and Hamphire, S., Silicon nitrid-silicon carbide nanocomposites prepared by water processing of comercially available powders. *Journal of the European Ceramic Society*, 1997, **17**, 1917–1923.